

ReaChR: a red-shifted variant of channelrhodopsin enables deep transcranial optogenetic excitation

John Y Lin^{1,5}, Per Magne Knutsen^{2,5}, Arnaud Muller², David Kleinfeld^{2,3} & Roger Y Tsien^{1,4}

Channelrhodopsins (ChRs) are used to optogenetically depolarize neurons. We engineered a variant of ChR, denoted red-activatable ChR (ReaChR), that is optimally excited with orange to red light (λ ~590–630 nm) and offers improved membrane trafficking, higher photocurrents and faster kinetics compared to existing red-shifted ChRs. Red light is less scattered by tissue and is absorbed less by blood than the blue to green wavelengths that are required by other ChR variants. We used ReaChR expressed in the vibrissa motor cortex to drive spiking and vibrissa motion in awake mice when excited with red light through intact skull. Precise vibrissa movements were evoked by expressing ReaChR in the facial motor nucleus in the brainstem and illumination with red light through the external auditory canal. Thus, ReaChR enables transcranial optical activation of neurons in deep brain structures without the need to surgically thin the skull, form a transcranial window or implant optical fibers.

ChRs are light-gated, non-specific cation channels that allow the selective depolarization of genetically targeted cells^{1–6}. However, currently available ChRs are limited by action spectra that typically peak at 450–545 nm^{7–11}. In mammalian systems, such blue-green wavelengths have limited penetration depths into neural tissue¹², as they are strongly absorbed by endogenous chromophores such as flavins, hemoglobin and melanin, and they are scattered more strongly than yellow-red wavelengths. A common means to circumvent this attenuation and achieve deep ChR excitation is to insert a thin optical fiber into the target neural tissue¹³. However, this invasive procedure requires precise stereotaxic positioning that may be difficult to perform when ChR is expressed in subcortical nuclei, and the fiber may damage neuronal and/or vascular structures *en route* to the target. The practical issue of efficient light delivery can be solved by creating a red-shifted ChR with spectral peaks near or above 600 nm, where light absorption by hemes and scattering cross-sections drop off steeply¹². Such ChRs could facilitate the stimulation of deep structures with a light source placed outside the tissue or region of interest and thus mitigate the need for invasive stimulation.

In this study, we engineered a new variant of ChR that we named ReaChR for red-activatable ChR. Compared to the previously described ChRs with red spectral shifts VChR1 (ref. 14) and C1V1^{E122T} (ref. 11), ReaChR has improved membrane trafficking

and expression in mammalian cells, a more robust spectral response above 600 nm and an enhanced steady-state response to light with wavelengths longer than 600 nm. When ReaChR was expressed in the mouse vibrissae motor cortex (vM1), we could trigger temporally precise neuronal responses by illumination of the cortical surface with 617 nm light through a transcranial window or evoke vibrissae movements through the intact skin and bone at wavelengths ranging from 470 to 655 nm. Expression of ReaChR in the facial motor nucleus of the brainstem allowed us to reliably activate vibrissa motoneurons with wavelengths up to 655 nm through the non-invasive placement of a light-emitting diode (LED) at the opening of the external auditory canal. Thus, ReaChR enables effective and temporally precise non-invasive stimulation of deep brain structures with ChR technology.

RESULTS

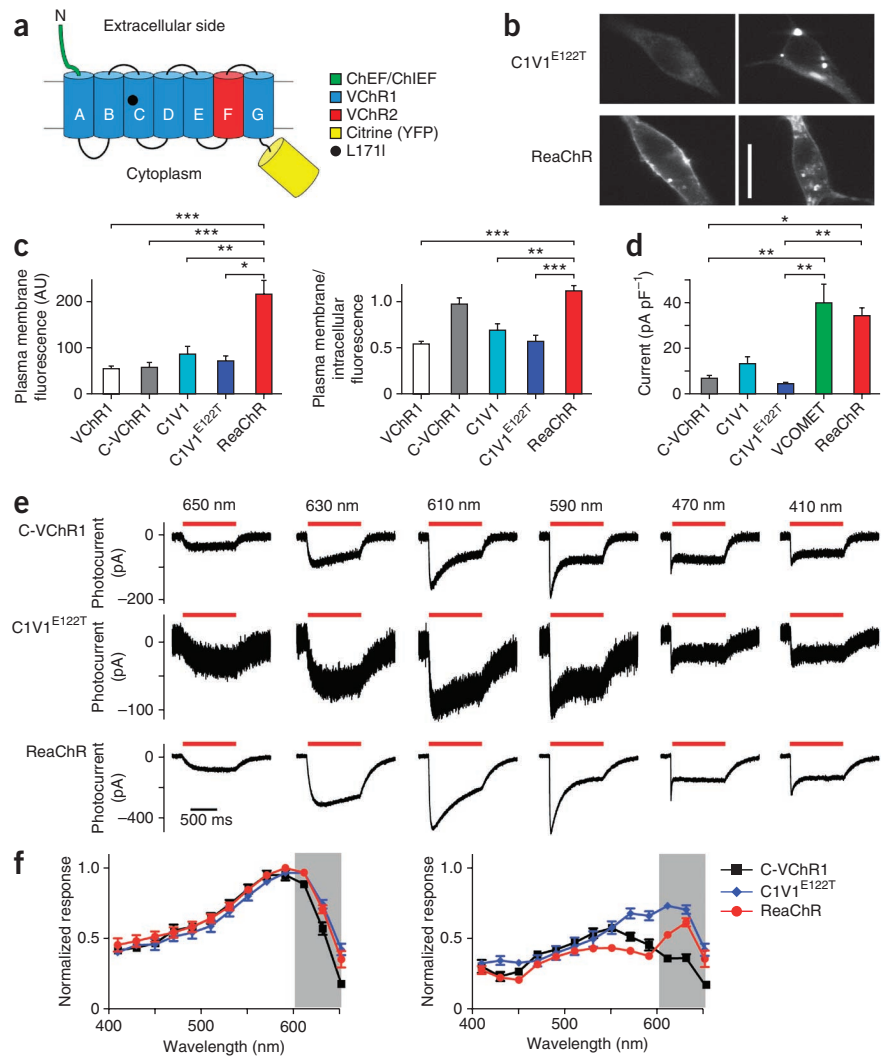
Development of a red-activatable ChR

The red-shifted ChR VChR1 (ref. 14), which has minimal trafficking to the membrane as well as poor expression in mammalian cells^{11,15}, served as a template to engineer an efficient red light-activated ChR. To improve membrane trafficking, we examined the superior membrane trafficking of the variant ChIEF⁷, which gives almost exclusive plasma membrane expression with minimal cytosolic aggregation in mammalian cells without the need for additional trafficking signals, unlike many other ChR variants (**Supplementary Fig. 1**)¹⁵. We thus replaced the N terminus of VChR1 before the first transmembrane domain with the corresponding ChIEF sequence. The new construct, denoted C-VChR1, had considerably improved membrane trafficking¹⁵ ($P < 0.001$ for VChR1 compared to C-VChR1). To increase the expression level, we replaced transmembrane domain F of VChR1 with the corresponding VChR2 helix, a strategy that has been shown previously to increase the expression level of ChR in ChR1-ChR2 chimeras¹⁶. This new variant, named VCOMET for VChR optimized for membrane expression and trafficking, had a red-shifted response spectra similar to that of C-VChR1 or VChR1¹⁵, with spectral peaks at 590 and 530 nm for the maximum and steady-state (also called plateau) responses, respectively (**Supplementary Fig. 2b**). VCOMET expressed strongly in mammalian cells and retained robust membrane trafficking (**Supplementary Fig. 1**). It also yielded greater photocurrent in HEK293 cells (39 ± 8 pA pF⁻¹ (mean \pm s.e.m.), $n = 13$) compared to C-VChR1 (6.9 ± 1.0 pA pF⁻¹, $n = 13$; $P < 0.01$) and comparable photocurrents to mammalian codon-optimized ChEF

¹Department of Pharmacology, University of California, San Diego, La Jolla, California, USA. ²Department of Physics, University of California, San Diego, La Jolla, California, USA. ³Section of Neurobiology, University of California, San Diego, La Jolla, California, USA. ⁴Howard Hughes Medical Institute, La Jolla, California, USA. ⁵These authors contributed equally to this work. Correspondence should be addressed to J.Y.L. (j8lin@ucsd.edu).

Received 3 June; accepted 29 July; published online 1 September 2013; doi:10.1038/nn.3502

Figure 1 Basic properties of ReaChR compared to those of C-VChR1 (VChR1 with the ChIEF N terminus) and C1V1^{E122T}. **(a)** Schematic design of ReaChR. ReaChR consists of the N terminus of the ChEF (or ChIEF) variant (ChEF/ChIEF), transmembrane domains A–E and G of VChR1, transmembrane domain F of VChR2 and the L171I point mutation. **(b)** Examples of C1V1^{E122T} and ReaChR expression in HEK293 cells as visualized by the fluorescence of fused Citrine. Much of the ReaChR expression was at the plasma membrane, whereas C1V1^{E122T} expression was more intracellular, with strong aggregation. Scale bar, 20 μm . **(c)** The relative plasma membrane expression level (left) and the ratio of plasma membrane to intracellular fluorescence (right) of VChR1 ($n = 19$), C-VChR1 ($n = 29$), C1V1 ($n = 26$), C1V1^{E122T} ($n = 16$) and ReaChR ($n = 21$) as measured with Citrine fluorescence. AU, arbitrary units. **(d)** The mean photocurrent amplitudes of C-VChR1 ($n = 13$), C1V1 ($n = 10$), C1V1^{E122T} ($n = 10$), VCOMET ($n = 13$) and ReaChR ($n = 9$) recorded from HEK293 cells. The current amplitudes were measured at the wavelengths that evoked the greatest response in each variant and were normalized to cell capacitance. The data in **c** and **d** are shown as the mean \pm s.e.m. * $P < 0.05$, ** $P < 0.01$, *** $P < 0.001$, Kruskal-Wallis test with *post-hoc* Dunn's test performed on all pairs of variants (only significant differences detected with Dunn's tests with VCOMET or ReaChR are shown; the statistical tests shown in **d** also include comparison to oChIEF ($n = 12$) and oChIEF ($n = 7$)). $H = 31.63$, $k = 5$, $P < 0.0001$ (**c**, left); $H = 41.28$, $k = 5$, $P < 0.0001$ (**c**, right); $H = 48.02$, $k = 7$, $P < 0.0001$ (**d**). **(e)** The responses of C-VChR1 (top), C1V1^{E122T} (middle) and ReaChR (bottom) to 650, 630, 610, 590, 470 and 410 nm light of the same photon flux (5.1×10^{16} photon $\text{mm}^{-2} \text{s}^{-1}$). **(f)** The spectra of the maximum response (left) and steady-state (plateau) response (right) of C-VChR1 ($n = 7$), C1V1^{E122T} ($n = 8$) and ReaChR ($n = 7$). The responses were normalized to the maximum response of each cell. The gray regions highlight the response above 600 nm. The data in **f** are shown as the mean \pm s.e.m.



(oChIEF; 48 ± 8 pA pF^{-1} , $n = 12$; **Supplementary Fig. 2a**) and mammalian codon-optimized ChIEF (oChIEF; 52 ± 7 pA pF^{-1} , $n = 7$). VCOMET had a reversal potential (12 ± 2 mV (mean \pm s.e.m.), $n = 8$) that was significantly higher than that of oChIEF (4 ± 1 mV, $n = 5$; $P < 0.05$) but not that of the calcium-translocating ChRs, CatChs¹⁷ (5 ± 1 mV, $n = 6$) in physiological saline ($H = 10.39$, $k = 4$, $P = 0.0155$ for comparisons between VCOMET, ChIEF, CatCh and ReaChR) and a reduced inward rectification similar to that of oChIEF (**Supplementary Fig. 2c**)⁷.

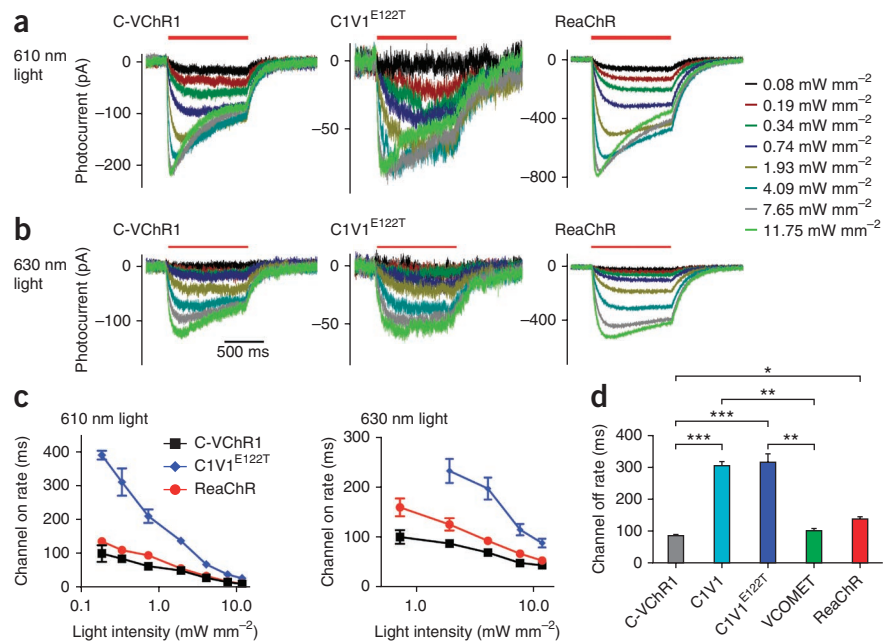
Although VCOMET responded strongly to light above 600 nm (**Supplementary Fig. 2b**), the responses at these longer wavelengths were desensitizing and did not recover completely in the dark without reconditioning with 410 nm light (**Supplementary Fig. 3**). We thus sought to reduce the desensitization of VCOMET to light above 600 nm through known point mutations of ChRs. The ChETA mutation¹⁷ did not red shift or reduce the desensitization of VCOMET. The corresponding H134R mutation of ChR2 (ref. 18) slowed the channel kinetics and thus degraded the temporal fidelity of the ChR. One mutation, L171I (**Fig. 1a**), which corresponds to the same position of the ChIEF mutation⁷, increased the amplitude of the photoresponse at both

610 and 630 nm light through reduced desensitization while retaining the membrane trafficking and expression of VCOMET (**Figs. 1** and **2** and **Supplementary Fig. 4**) and thus led to an increase in the steady-state (plateau) spectral peak at 630 nm (**Fig. 1f**). This formed ReaChR, the new ChR. ReaChR retained the reversal potential (7 ± 4 mV, $n = 6$), reduced inward rectification and photocurrent amplitude (34 ± 4 pA pF^{-1} , $n = 9$) of VCOMET (**Fig. 1b–d**). The one limitation of ReaChR relative to C-VChR1 was the slower channel closure rate after termination of the light pulse: $\tau_{1/e} = 137 \pm 7$ ms (mean \pm s.e.m. $n = 11$) for ReaChR compared to $\tau_{1/e} = 85 \pm 4$ ms ($n = 9$) for C-VChR1 ($P < 0.05$) (**Fig. 2d** and **Table 1**).

Comparisons of red-shifted ChR variants in cell culture

The ChR variant C1V1^{E122T} has been shown to excite the neuronal membrane potential with 630 nm light that is pulsed for 50 ms¹¹. To gauge the potential benefit of ReaChR over C1V1 and related constructs, we characterized the attributes of ReaChR in comparison to those of C1V1, C1V1^{E122T} and VCOMET (**Table 1**). C1V1 and C1V1^{E122T} both expressed strongly in HEK293 cells as visualized with Citrine¹⁹ fluorescence of the C-terminal fusion protein. However,

Figure 2 Kinetics of C-VChR1, C1V1^{E122T} and ReaChR. (a) Representative responses of a C-VChR1-expressing (left), a C1V1^{E122T}-expressing (middle) and a ReaChR-expressing (right) HEK293 cell to 0.08, 0.19, 0.34, 0.74, 1.93, 4.09, 7.65 and 11.75 mW mm⁻² of 610 nm light. (b) The responses of the same cells as in a to 630 nm light of varying intensities. (c) Channel onset time constants of C-VChR1 (*n* = 10), C1V1^{E122T} (*n* = 6) and ReaChR (*n* = 10) to 610 nm (left) and 630 nm (right) light of different intensities. Data are shown as the mean ± s.e.m. (d) Channel closure time constants of C-VChR1 (*n* = 11), C1V1 (*n* = 6), C1V1^{E122T} (*n* = 8), VCOMET (*n* = 9) and ReaChR (*n* = 11). **P* < 0.05, ***P* < 0.01, ****P* < 0.001, Kruskal-Wallis test with *post-hoc* Dunn's multiple comparison tests on all pairs of variants (*H* = 36.76, *k* = 5, *P* < 0.0001). Data are shown as the mean ± s.e.m.



neither C1V1 nor C1V1^{E122T} trafficked to the membrane as well as ReaChR or VCOMET in these cells, and they both showed high amounts of intracellular aggregation and strong cytosolic fluorescence (Fig. 1b,c). The mean photocurrent of C1V1 expressed in HEK293 cells (13 ± 3 pA pF⁻¹, *n* = 10) was smaller than those for VCOMET and ReaChR (Fig. 1d), possibly because of reduced efficiency in trafficking to the plasma membrane (Fig. 1c). Introduction of the E122T mutation to form C1V1^{E122T} reduced the C1V1 photocurrent ~66% (4 ± 1 pA pF⁻¹, *n* = 10; Fig. 1d), although its action spectrum was red shifted, with peaks at 590 and 610 nm for the maximum and steady-state (plateau) responses, respectively (Fig. 1e,f). The channel kinetics of C1V1^{E122T} were significantly slower than those of VCOMET and C-VChR1, with a channel closure time constant of $\tau_{1/e}$ = 315 ± 26 ms (*n* = 8), although this value is similar to that of the parent construct, C1V1 ($\tau_{1/e}$ = 306 ± 10 ms, *n* = 6; Fig. 2d). The activation kinetics of C1V1^{E122T} were also 1.5- to 3-fold slower than ReaChR and C-VChR1 at the same light intensities for 610 and 630 nm light (Fig. 2c). However, the photocurrent amplitudes of C-VChR1, ReaChR and C1V1^{E122T} showed similar functional forms in response to incident light intensity (Supplementary Fig. 4). With C-VChR1, C1V1^{E122T} and ReaChR, increasing the stimulation intensity of 610 nm light led to reduction of the steady-state (plateau) response amplitudes at higher light intensities (Fig. 2a and

Supplementary Fig. 4). As ReaChR has improved membrane trafficking, greater photocurrents and faster kinetics compared to C1V1^{E122T}, we propose that ReaChR is a robust means to stimulate neurons with red-orange to red light.

Comparison of ChR variants in cultured neurons

We compared the properties of ReaChR with those of other ChR variants in cultured neurons²⁰. ReaChR traffics to the membrane well and expresses strongly in neurons (*n* = 22), as we observed in HEK293 cells (Fig. 3a). The variants C1V1^{E122T} (*n* = 13) and C1V1^{E122T} with an additional trafficking sequence, denoted C1V1^{E122T}-TS (*n* = 17)^{11,20}, trafficked to the membrane as well as ReaChR in cultured neurons (Fig. 3a,b), which is in contrast to the relatively greater trafficking that we observed for ReaChR in HEK293 cells. However, the expression levels of C1V1^{E122T} and C1V1^{E122T}-TS were approximately 80–84% lower than those of ReaChR under identical conditions (Fig. 3a,b). We observed occasional cells with high expression levels of C1V1^{E122T} and C1V1^{E122T}-TS, although they occurred too infrequently to be of general utility.

In order to compare the photocurrent amplitudes of different ChR variants, we used a titer-matched lentivirus with a truncated human synapsin 1

Table 1 Comparisons of the channel kinetics and properties of C-VChR1, VCOMET, ReaChR, C1V1 and C1V1^{E122T}

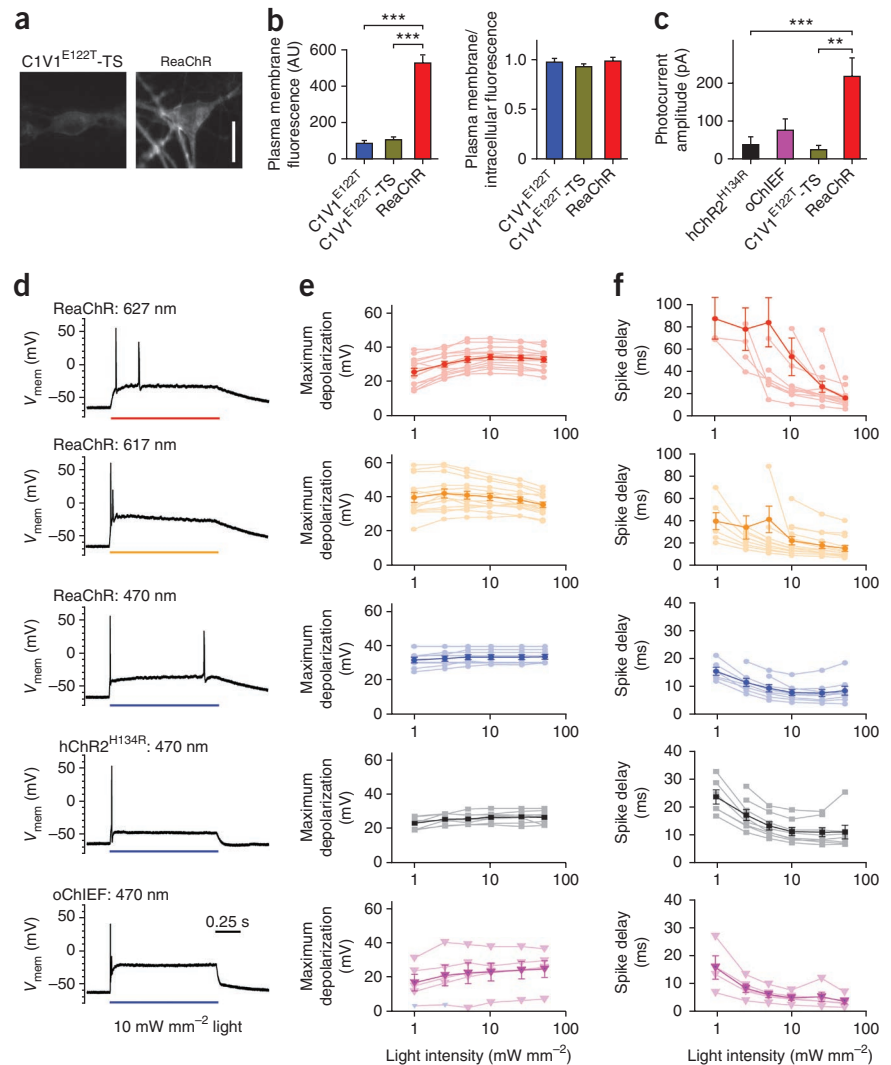
Variant	Response spectra (nm)		Mean membrane fluorescence (AU)	Mean ratio of membrane to cytosol fluorescence	Mean photocurrent (pA pF ⁻¹)	Channel on rate, 610 nm	Channel on rate, 630 nm	Channel off rate, $\tau_{1/e}$ (ms)
	Maximum	Steady state				$\tau_{1/e}$ (ms), 610 nm at 7.6 mW mm ⁻²	$\tau_{1/e}$ (ms), 630 nm at 7.6 mW mm ⁻²	
C-VChR1	~570	~550	58 ± 11 (<i>n</i> = 29)	0.98 ± 0.07 (<i>n</i> = 29)	6.9 ± 1.1 (<i>n</i> = 13)	19.4 ± 0.8 (<i>n</i> = 11)	49.4 ± 2.0 (<i>n</i> = 10)	84.9 ± 3.9 (<i>n</i> = 11)
VCOMET	~590	~530	ND	1.10 ± 0.07 (<i>n</i> = 26) ^a	38.9 ± 7.8 (<i>n</i> = 13)	ND	ND	100.4 ± 6.6 (<i>n</i> = 9)
ReaChR	~590	~630	218 ± 29 (<i>n</i> = 21)	1.12 ± 0.07 (<i>n</i> = 21)	33.5 ± 3.6 (<i>n</i> = 9)	20.7 ± 0.6 (<i>n</i> = 11)	68.1 ± 4.2 (<i>n</i> = 10)	137.2 ± 7.1 (<i>n</i> = 11)
C1V1	ND	ND	87 ± 17 (<i>n</i> = 26)	0.70 ± 0.06 (<i>n</i> = 26)	13.0 ± 3.0 (<i>n</i> = 10)	ND	ND	306.3 ± 10.3 (<i>n</i> = 6)
C1V1 ^{E122T}	~600	~610	72 ± 11 (<i>n</i> = 16)	0.58 ± 0.06 (<i>n</i> = 16)	4.4 ± 0.6 (<i>n</i> = 10)	41.5 ± 4.6 (<i>n</i> = 7)	115.8 ± 11.1 (<i>n</i> = 6)	315.4 ± 26.0 (<i>n</i> = 8)

Electrophysiological characterizations were made under voltage-clamp recordings in HEK293 cells in which the membrane potential could be accurately clamped at -60 mV. Plasma membrane and intracellular fluorescence were measured in HEK293 cells transiently expressing ChR fused to Citrine imaged with a confocal laser-scanning microscope. ND, not determined; AU, arbitrary units.

^aThe value of VCOMET was acquired in a separate experiment with different pixel-dwelling time settings.



Figure 3 Characterization and comparison of different ChR variants in primary cultured hippocampal neurons. **(a)** Representative confocal images of neurons expressing C1V1^{E122T}-TS-Citrine (C1V1^{E122T}-TS) or ReaChR-Citrine (ReaChR). Scale bar, 20 μm . **(b)** Quantification of plasma membrane fluorescence (left) and the ratio of plasma membrane to cytosolic fluorescence (right) of C1V1^{E122T}-Citrine ($n = 13$), C1V1^{E122T}-TS-Citrine ($n = 17$) and ReaChR-Citrine ($n = 22$). **(c)** Photocurrent amplitudes of primary cultured neurons expressing hChR2^{H134R} ($n = 16$), oChIEF ($n = 17$), C1V1^{E122T}-TS ($n = 14$) or ReaChR ($n = 16$) as measured with voltage-clamping recordings. The hChR2^{H134R}- and oChIEF-expressing neurons were stimulated with 10 mW mm^{-2} of 470 nm light, and the C1V1^{E122T}-TS-expressing and ReaChR-expressing neurons were stimulated with 10 mW mm^{-2} light at 590 nm. The data in **b** and **c** are shown as the mean \pm s.e.m. $**P < 0.01$, $***P < 0.001$, Kruskal-Wallis test with *post-hoc* Dunn's multiple comparison tests on all pairs of variants. $H = 37.66$, $k = 3$, $P < 0.0001$ (**b**, left); $H = 1.09$, $k = 3$, $P = 0.58$ (**b**, right); $H = 18.32$, $k = 4$, $P = 0.0004$ (**c**). **(d)** Representative recordings of neurons expressing different ChR variants to 1 s of 10 mW mm^{-2} of LED light of the indicated wavelengths under current-clamp recordings. Depolarization of membrane potential (V_{mem}) is indicated with upward inflections of the traces. **(e)** Quantification of the amounts of light-induced depolarization in neurons expressing the different variants to light of increasing intensities. **(f)** Quantification of the action potential latencies from the onset of the light pulse to increasing intensities of light. The lighter colored traces in **e** and **f** are the responses of individual cells, and the darker colored traces are the mean \pm s.e.m.



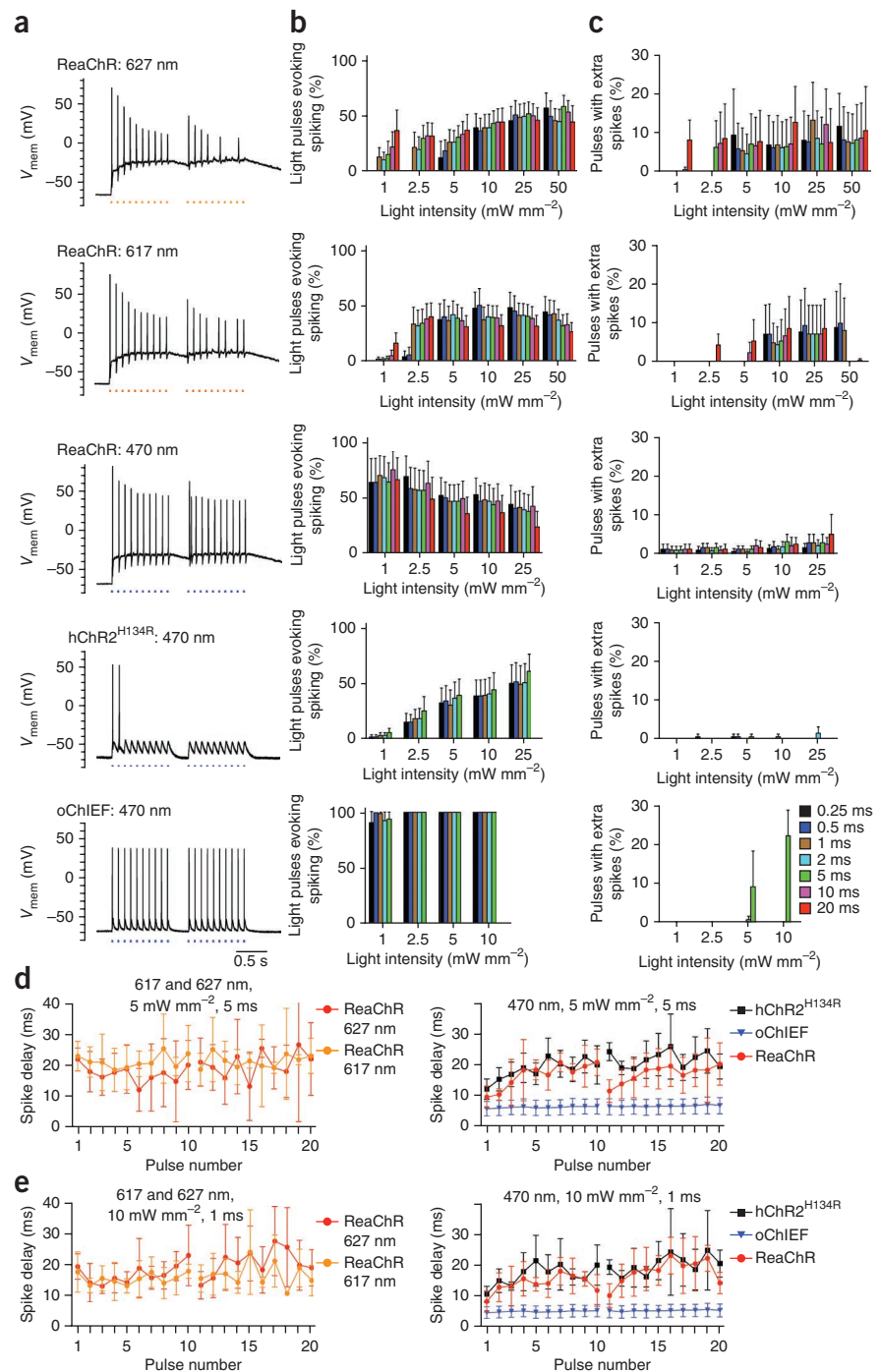
promoter (hSyn) to express enhanced yellow fluorescent protein-tagged human codon-optimized ChR2^{H134R} (hChR2^{H134R}-eYFP), oChIEF-Citrine, C1V1^{E122T}-TS-Citrine and ReaChR-Citrine in cultured neurons. We selected cells for recording on the basis of their morphology under bright-field visualization. We did not use fluorescence signal-based selection or the selective α -CamKII α promoter²⁰ to avoid bias in the selection process. In all cases, ChRs were activated by 10 mW mm^{-2} of light at the respective maximum response wavelengths. We recorded the photocurrents under voltage clamp. We observed that currents from ReaChR-Citrine-expressing cells (219 ± 50 pA, $n = 16$) were greater than those from hChR2^{H134R}-expressing (37 ± 21 pA, $n = 16$) and C1V1^{E122T}-TS-expressing (23 ± 11 pA, $n = 14$) neurons but were non-significantly greater than those from oChIEF-expressing neurons (75 ± 31 pA, $n = 17$) (**Fig. 3c**). None of the ReaChR-expressing cells tested were unresponsive to light, whereas many hChR2^{H134R}-expressing ($n = 9$) and C1V1^{E122T}-TS-expressing ($n = 5$) neurons had no detectable response to light.

To test the utility of ReaChR to induce suprathreshold depolarization in neurons, we recorded cells under a current clamp without blockers of voltage-gated channels. We injected current through the patch pipette to maintain the membrane potentials of all cells at -65 mV; we did not correct junction potentials. In ReaChR-expressing neurons, we were able to achieve suprathreshold depolarization

with blue (470 nm), red-orange (617 nm) and red light (627 nm) in response to 1s light pulses (**Fig. 3d**). The amount of depolarization and the spike-delayed time were dependent on wavelength, light intensity and expression level, in addition to the membrane properties of the neurons (cell type, membrane resistance and capacitance). Cells expressing ReaChR retained normal morphological appearances and physiological membrane properties (**Supplementary Fig. 5**), suggesting minimal toxic effects with expression. With 617 nm light, we were able to achieve 25–45 mV depolarization (mean, 35 mV) in the expressing cells (**Fig. 3e**) and trigger action potentials with a 7–40 ms delay time (mean, 15 ms; **Fig. 3f**) when stimulated at a high light intensity ($n = 14$). With 627 nm light, we were able to achieve 24–44 mV depolarization (mean, 34 mV; **Fig. 3e**) and spike delays of 7–35 ms (mean, 17 ms; **Fig. 3f**) ($n = 14$). Blue light at 470 nm was also effective in achieving suprathreshold depolarization of ReaChR-expressing cells, with depolarization of 30–40 mV (mean, 34 mV; **Fig. 3e**) and a spike delay of 4–19 ms (mean, 9 ms; **Fig. 3f**) ($n = 8$). In comparison, the maximum depolarization achieved in neurons expressing hChR2^{H134R} was 22–32 mV (mean, 26 mV; **Fig. 3e**), and the spike delay ranged from 7 to 25 ms (mean, 11 ms) (**Fig. 3f**) ($n = 8$). In oChIEF-expressing neurons, the amount of depolarization was 8–38 mV (mean, 26 mV; **Fig. 3e**), and the spike delay ranged from 1.6 to 7 ms (mean, 8 ms; **Fig. 3f**) when stimulated with 470 nm light ($n = 5$).



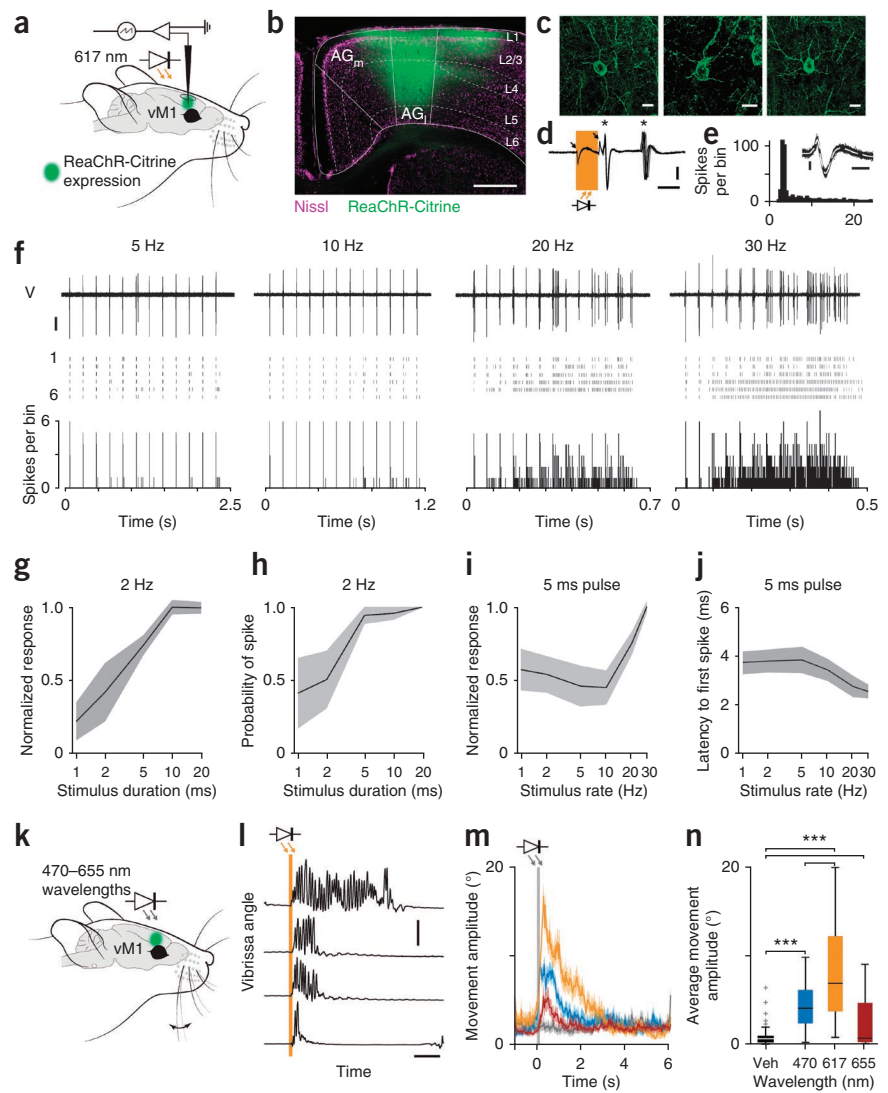
Figure 4 The responses of neurons expressing the different ChR variants to a 10 Hz pulsed-light stimulation train. **(a)** Example recordings of neurons expressing the indicated ChR variants to 10 Hz of light stimulation at 10 mW mm⁻² of 1 ms duration. Two ten-pulse trains 250 ms apart were used to simulate two bursting episodes. Currents were injected to sustain the resting membrane potential at -65 mV. **(b)** The percentage of pulses resulting in action potentials of varying light intensities and pulse durations recorded from neurons expressing the different variants. **(c)** Percentage of pulses resulting in extra action potentials of varying light intensities and pulse durations of the different variants. For 627 nm stimulation of ReaChR in **b** and **c**, *n* = 5–12 for each of the conditions. For 617 nm stimulation of ReaChR in **b** and **c**, *n* = 3–11. For 470 nm stimulation of ReaChR in **b** and **c**, *n* = 4–8. For stimulation of hChR2^{H134R} in **b** and **c**, *n* = 7–8. For the stimulation of oChIEF in **b** and **c**, *n* = 5–7 (see also **Supplementary Data Set 1**). The data in **b** and **c** are shown as the mean ± s.e.m. **(d,e)** Summaries of the mean latencies and s.d. of the light-triggered action potentials of each pulse in ReaChR-, hChR2^{H134R}- and oChIEF-expressing neurons to the indicated wavelengths, intensities and durations. Pulses that did not trigger action potentials were not included in the analysis. For 627 nm stimulation of ReaChR in **d** and **e**, 7 and 8 cells were tested, respectively. Each data point in **d** and **e** is the mean of 2–6 and 3–6 values, respectively. For 617 nm stimulation of ReaChR in **d** and **e**, 8 and 9 cells were tested, respectively. Each data point in **d** and **e** is the mean of 2–6 and 1–6 values, respectively. For 470 nm stimulation of ReaChR in **d** and **e**, 8 cells were tested, and each data point is the mean of 2–8 values. For the stimulation of hChR2^{H134R} in **d** and **e**, 8 cells were tested, and each data point is the mean of 2–8 values. For the stimulation of oChIEF in **d** and **e**, 6 cells were tested, and each data point is the mean of 6 values (see also **Supplementary Data Set 1**). The data in **d** and **e** are shown as the mean ± s.d.



Pulsed illumination at 10 Hz was an effective trigger for spiking in ReaChR-expressing neurons at 470, 617 and 627 nm (**Fig. 4a**). Light pulses of weak intensity and short duration often lead to loss of temporal fidelity from insufficient depolarization (**Fig. 4b**). Light pulses of too high an intensity lead to extra action potentials and depolarization block as a result of insufficient repolarization between light pulses, which were the main reasons for the loss in temporal fidelity that we observed (**Fig. 4c**). In addition to stimulation intensity and pulse duration, cell membrane properties and the expression level of ReaChR also affect the ability to trigger action potentials in response to pulsed light. Thus, one specific stimulation protocol that achieved complete fidelity in one ReaChR-expressing cell, for example, 0.5 ms of 5 mW mm⁻² of 617 nm light or 1 ms of 10 mW mm⁻² of 627 nm light, could fail to trigger action potentials in another cell with different membrane properties and expression levels. We observed this same phenomenon with stimulation at 5 Hz (**Supplementary Fig. 6**).

With regard to the fidelity of spike generation in neurons with ChR variants other than ReaChR, we observed lower firing reliabilities with hChR2^{H134R}-expressing cells in response to 470 nm light. This variant introduced a high amount of channel desensitization that led to subthreshold depolarization with light pulses toward the end of a pulse train (**Fig. 4a**). As the overall amount of depolarization that we observed with hChR2^{H134R} was lower, extra spiking was rare. Cells expressing oChIEF had the highest temporal precision, as measured by the percentage of pulses achieving suprathreshold depolarization, the shortest spike delay and a variability in spike latency (**Fig. 4b–e**), and this higher fidelity was sustained at higher stimulation frequencies (**Supplementary Fig. 6**). Yet even with oChIEF, we observed

Figure 5 *In vivo* expression and utilization of ReaChR for cortical control. (a) Schematic of vM1 stimulation and recording. ReaChR was expressed in vM1 and visualized by Citrine fluorescence (green). vM1 was exposed for electrophysiology, and ReaChR-expressing neurons were activated with 617 nm light. (b) Coronal section through the medial (AG_m) and lateral (AG_l) agranular vM1 of an infected mouse showing ReaChR expression (green). Neurons were counterlabeled with a fluorescent marker (NeuroTrace; magenta). Scale bar, 500 μ m. (c) ReaChR-expressing neurons in vM1. Scale bars, 10 μ m. (d) Photoactivated spikes in a ReaChR-expressing neuron recorded *in vivo* during anesthesia (recording depth, 410 μ m). Single 2 ms pulses of 617 nm light (orange bar) evoked one or more spikes (indicated by asterisks; $n = 12$ pulses at 2 Hz). Arrows indicate low-amplitude artifacts associated with the light switching on and off. Vertical scale bar, 100 μ V; horizontal scale bar, 2 ms. (e) Spike interval histogram and waveforms (inset) of the same unit demonstrating the unit as a single neuron. Vertical scale bar, 100 μ V; horizontal scale bar, 0.5 ms. (f) A ReaChR-expressing neuron activated with 2 ms pulses of 617 nm light at 5, 10, 20 and 30 Hz (12 pulses). Top, voltage trace during a train of 12 pulses (vertical scale bar, 100 μ V). Middle, rasters of spikes during six trains. Bottom, peristimulus time histogram of spikes across all trains. (g,h) Spikes per pulse (normalized to the maximum number of spikes evoked by the light pulses of the indicated duration; g) and probability of one or more evoked spikes (h) across a population of ReaChR-expressing neurons ($n = 8$) as a function of pulse duration (2–20 ms; pulse rate, 2 Hz). (i,j) Number of spikes per pulse (normalized to the maximum as in g; i) and the latency to the first spike (j) in neurons as a function of stimulus rate (1–30 Hz; pulse duration, 5 ms). (k) Schematic of *in vivo* activation of vM1 with ReaChR (green) through intact skin and bone of awake mice. Vibrissae movements were measured with high-speed video. (l) Traces of vibrissae movements in response to single 100 ms pulses (orange arrows and bar) of 617 nm light emitted by an LED placed 10 mm above the skin. Increasing values denote vibrissae protraction. Vertical scale bar, 40°; horizontal scale bar, 1 s. (m) Absolute movement amplitudes evoked by 100 ms pulses of 470, 617 and 655 nm light through intact skin in ReaChR-expressing mice ($n = 3$ mice, ten stimulus repetitions per condition per mouse). Additionally, three mice injected with viral vehicle solution (mock control) were stimulated through the skin with 617 nm light (black). (n) Boxplots of movements during the first second after vM1 photoactivation through the intact skull of mock-transduced (veh, black; $n = 3$ mice; 617 nm illumination) and ReaChR-expressing mice ($n = 3$ mice; 470–655 nm wavelengths). Vertical lines indicate the data range, boxes indicate the 25th to 75th percentile ranges, and the central lines mark the median. *** $P < 0.001$, one-sided Kolmogorov-Smirnov test. The light intensity used in a–n was 100 mW.



extra action potentials after strong depolarization in cells with high expression. The spike latency and variability were similar between ReaChR and hChR2^{H134R}, with a higher variability in the responses to stimulation pulses present later in the pulse train.

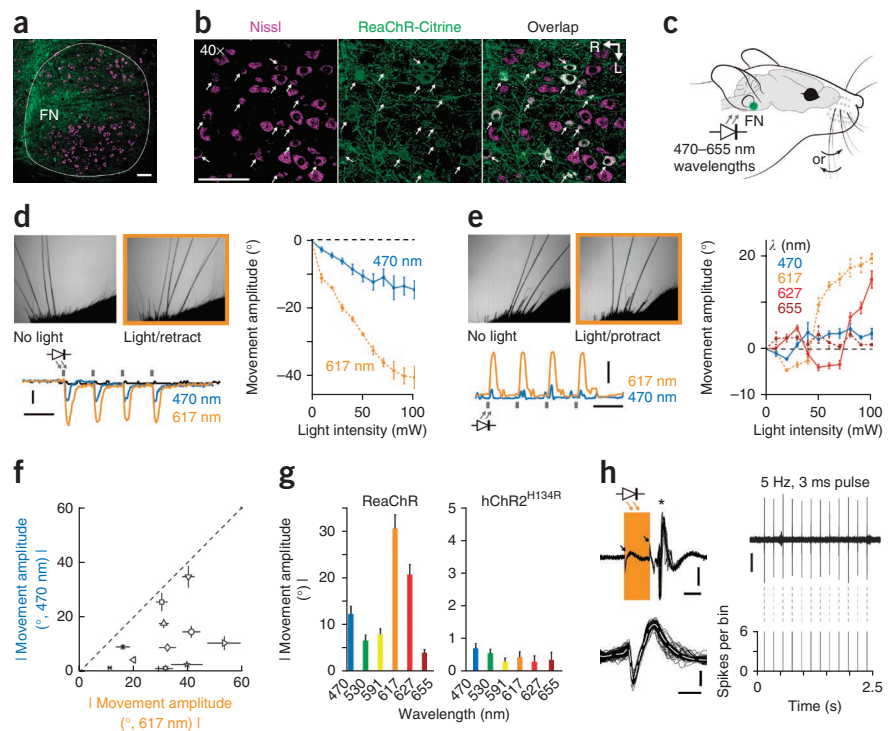
Excitation of ReaChR-expressing neurons *in vivo*

As red light can penetrate mammalian tissues *in vivo* with less attenuation compared to blue or green light¹², we used ReaChR to stimulate deep brain structures *in vivo*. We targeted two areas for *in vivo* stimulation: vM1, which is involved in the control and execution of vibrissa motion²¹, and the facial motor nucleus of the seventh cranial nerve, whose motoneurons innervate the muscles that are responsible for vibrissa movements. We incorporated ReaChR-Citrine

into a recombinant adeno-associated virus (rAAV) with a hSyn promoter and injected it into either vM1 or the facial motor nucleus of individual mice.

We confirmed ReaChR expression in vM1 3 weeks after injection. We head fixed the mice and monitored vibrissae movements with high-speed video either during light anesthesia with 1.0–1.5% (vol/vol) isoflurane or while the mice were awake (Fig. 5). For electrophysiological recordings, we removed the bone over vM1, mapped the zone of infection with epifluorescence imaging of the cortical surface and positioned a 617 nm LED 10 mm above the surface of the brain (Fig. 5a,b). We used short pulses of light, 1–20 ms in duration, to activate ReaChR-expressing neurons (Fig. 5c) and evoke spikes, as recorded extracellularly (Fig. 5d–f). ReaChR-expressing vM1 neurons

Figure 6 *In vivo* expression and utilization of ReaChR for brainstem activation. (a) Horizontal section through the facial motor nucleus (FN, indicated by the white outline) showing ReaChR-expressing neurons and the associated processes (green). Cells were labeled with a fluorescent marker (NeuroTrace; magenta). (b) Confocal images of ReaChR-expressing motoneurons (arrows). Scale bars (a,b), 100 μ m. R, rostral; L, lateral. (c) Schematic of an awake mouse expressing ReaChR in the facial motor nucleus photoactivated by LEDs placed at the opening of the external auditory canal. Vibrissae movements were recorded with high-speed video. (d) Vibrissae movements evoked by stimulating the facial motor nucleus in a ReaChR-expressing mouse. Left, video frames (top) showing vibrissae in the reference protracted position (no light) and at the peak retraction during photoactivation (light/retract) and traces of movements (bottom) in response to 470 and 617 nm light. The black trace indicates the movement of contralateral C2 vibrissa. Vertical scale bar, 100 ms light pulse (100 mW light output); horizontal scale bars, 10° and 1 s. Right, movement amplitude as a function of light output power. (e) Vibrissa movements evoked by stimulating the facial motor nucleus in a separate ReaChR-expressing mouse. Left, video frames (top) showing vibrissae in the reference retracted position (no light) and at peak protraction during stimulation (light/protract) and traces of movements (bottom) in response to 470 and 617 nm light. Right, movement amplitude as a function of light output power. Vertical scale bar, 100 ms light pulses (100 mW light output); horizontal scale bar, 10° and 1 s. (f) Population data of the absolute movement amplitudes evoked by 470 and 617 nm through-ear illumination (100 ms pulses at 1 Hz; $n = 12$ mice). (g) Comparison of the movement amplitudes evoked with light between 470 and 655 nm in ReaChR-expressing (left; $n = 12$ mice) and hChR2^{H134R}-expressing (right; $n = 3$ mice) mice (100 mW light output). Movement amplitudes at the same wavelengths were larger in ReaChR- compared to hChR2^{H134R}-expressing mice ($P < 0.001$, Kolmogorov-Smirnov test). (h) *In vivo* recording of a single unit in the facial motor nucleus region (based on stereotaxic coordinates) during photoactivation with 617 nm light (100 mW light output). Top left, voltage trace aligned to a 3 ms light pulse (orange bar; $n = 12$ pulses). Small artifacts are associated with the light pulses switching on and off (arrows). A single spike was evoked after each pulse (asterisk) with low temporal jitter and short latency (4 ms), suggesting that the unit expressed ReaChR and was directly activated. Vertical scale bar, 100 μ V; horizontal scale bar, 2 ms. Bottom left, overlapped spikes from the same unit demonstrating this as a single neuron. The unit was not spontaneously active and fired a single spike in response to the light pulse. Vertical scale bar, 100 μ V; horizontal scale bar, 0.5 ms. Top right, voltage trace recorded during a single train of 12 light pulses (vertical scale bar, 100 μ V). Middle right, rasters of spikes during six trains. Bottom right, peristimulus time histogram of spikes across all trains. The data in d,e,f and g are shown as the mean \pm s.e.m.



were reliably photoactivated at short latencies and with low temporal jitter (Fig. 5d). The evoked activity of a representative cortical single unit is shown in Figure 5d–f. This unit, which probably expressed ReaChR, fired one or more spikes in response to 2 ms pulses with submillisecond jitter and a short, 2.4 ms spike latency. The unit was reliably activated with trains of light pulses that ranged from 5 to 30 Hz. Increasing the rate of optical activation to greater than 20 Hz resulted in a larger number of extra spikes per pulse (Fig. 5f). We observed a monotonic increase in the number of evoked spikes and in the spiking probability as a function of stimulus duration ($n = 8$ single units; Fig. 5g,h). The spiking probability was above 0.95 when the stimulus duration was 5 ms or longer (Fig. 5h). When the stimulus rate exceeded 10 Hz, the population response increased ($P = 0.002$, one-sided Kolmogorov-Smirnov test; Fig. 5i) and the latency to the first spike decreased ($P = 0.01$, one-sided Kolmogorov-Smirnov test; Fig. 5j); these effects probably result from the slow closing kinetics of ReaChR.

Consistent with *in vivo* neural activation of ReaChR-expressing neurons, we found that vibrissae movements could be elicited by LED illumination in awake mice (Fig. 5k–n). Removal of skin and bone was not required to evoke these movements, and placing the stimulating LEDs 10 mm above the fur line was sufficient in all

cases (Fig. 5k). Movements were elicited with both blue (470 nm) and red (617 and 655 nm) illumination. Evoked movements were characteristic of those observed with electrical stimulation of vM1, showing both a rapid component^{22,23} and a sustained period, albeit with unpredictable duration, of rhythmic whisking that outlasted the stimulus²⁴ (Fig. 5l,m).

Our *in vivo* cortical experiment demonstrated stronger evoked movement responses to 617 nm as compared to 470 nm light ($P < 0.0001$, one-sided Kolmogorov-Smirnov test; Fig. 5m,n), which is consistent with the larger responses to orange-red light that we observed in cultured HEK293 cells (Fig. 1f and Supplementary Fig. 7) and the greater attenuation of blue compared to red light in mammalian tissue¹². We confirmed that these movements were caused by photoactivation of ReaChR by comparison with movements measured in a cohort of mock-transduced mice injected with a viral vehicle (Fig. 5m,n). Because we were able to evoke movements with 470 nm light in ReaChR-expressing mice, we tested whether movement could be evoked non-invasively with a standard blue light-activated ChR variant. We thus expressed hChR2^{H134R}-eYFP in vM1 with an identical rAAV vector and viral titer. Vibrissa movements could be evoked in mice expressing hChR2^{H134R} in vM1 with 470 nm light illumination ($n = 3$), but these movements were more infrequent, notably smaller

and shorter lasting compared to the movements evoked with 617 nm light in ReaChR-expressing mice (**Supplementary Fig. 7c–f**).

The durations and amplitudes of the movements evoked by vM1 stimulation in ReaChR-expressing mice were unpredictable (**Fig. 5I**), mirroring the results obtained with electrical stimulation in awake mice²⁴ but nonetheless complicating comparisons of different stimulation parameters. As a more stringent test of the sensitivity of ReaChR to different wavelengths *in vivo*, we targeted ReaChR to the mystacial motoneurons in the facial motor nucleus of the brainstem that directly control vibrissa movements (**Fig. 6a,b**). It has been shown previously that in deeply anaesthetized mice, direct electrical stimulation of these neurons can reliably drive vibrissa movements, producing a relatively noise-free and controlled behavioral output²⁵. In mice, the facial motor nucleus is located at a depth of up to 6 mm in the ventral part of the brainstem. We delivered light at 470, 530, 591, 617, 627 and 655 nm wavelengths in a non-invasive manner by placing an LED at the opening of the external auditory canal, thus illuminating the brainstem at a distance of 8–10 mm from the midline through intact tissue and bone (**Fig. 6c**). The external ear canal provides a convenient anchor point for non-invasive LED placement, bypasses fur and provides an opportunity to limit photoactivation to one side of the brainstem. We typically flashed the LEDs for periods of 100 ms at 1 Hz with a 1–100 mW light output; we found no visual indications of any heat-related damage to the outer ear tissue. Activation of ReaChR-expressing neurons elicited highly reproducible and temporally precise vibrissae movements, which is consistent with the direct activation of motoneurons (**Fig. 6d,e** and **Supplementary Video 1**). Although a topographic organization of the facial muscle representation within the facial motor nucleus has been documented, the exact distribution of all the motoneurons innervating muscles that are involved in vibrissa control is not known²⁶. Both protraction and retraction of the vibrissae are actively controlled by multiple extrinsic and intrinsic muscles^{22,27}. We found no consistent pattern between the intrafacial motor nucleus locations of infected motoneurons and the evoked movement trajectories, and in several mice, both net protraction and retraction could be elicited by adjusting the light intensity appropriately (**Fig. 6d,e**). As an example, **Figure 6d** shows evoked movements in a mouse in which light stimulation led to the retraction of all vibrissae independently of light intensity (10–100 mW light output, 100 ms pulses; **Supplementary Video 2**). Evoked retractions were three times larger when ReaChR was activated at 617 nm as compared to 470 nm (40° compared to 13°, respectively, at maximum amplitude). Similarly, light stimulation of a different mouse (**Fig. 6e**) produced sixfold larger movements at 617 nm compared to 470 nm (19° compared to 3°, respectively, at maximum amplitude). We observed this pattern of stronger activation at 617 nm compared to 470 nm in all ReaChR-expressing mice (**Fig. 6f**).

Vibrissa movements in ReaChR-expressing mice could be evoked across a broad range of wavelengths, which is consistent with our *in vitro* results. The largest movements were evoked at 617 nm, followed by 627 nm and 470 nm. Smaller vibrissa movements were also evoked with 530, 591 and 655 nm illumination (**Fig. 6g**). We confirmed that these movements resulted from photoactivation of ReaChR and not LED-related heating of neural tissue or visually evoked responses by the fact that we did not observe any movement in a cohort of mice expressing the blue light-activated hChR2^{H134R} channel in the facial motor nucleus ($n = 15$; **Fig. 6g** and **Supplementary Fig. 7g–i**) and by recording single units in the brainstem of ReaChR-expressing mice that reliably responded with short latencies and submillisecond temporal jitter to light stimulation (**Fig. 6h**).

The variability in whisking between individual mice in response to illumination of the facial motor nucleus was great (**Fig. 6f**). This was probably caused by variations in the exact locations of ReaChR-expressing motoneurons within the facial motor nucleus, which is ~1 mm in width, and/or high expression levels in individual motoneurons that resulted in very low spiking thresholds. In principle, this variability could also be caused by direct stimulation of the facial motor nerve. We confirmed that motoneuron axons were labeled with ReaChR-Citrine and that vibrissa movements could also be evoked by direct illumination of the peripheral motor nerve through the skin of the lower cheek. These movements, however, were smaller and of shorter duration than those evoked through the ear (**Supplementary Fig. 7a**). In addition, movements were not evoked when stimulating through the ear contralateral to the side of ReaChR expression (617 nm, 100 mW light output), which shows that the lateralization of optogenetically evoked brainstem activity can be controlled with through-skull stimulation (**Supplementary Fig. 7b**).

DISCUSSION

The optimal wavelength range for optical imaging into mammalian tissue is near infrared (600–1,300 nm), where light scattering decreases with increasing wavelength and absorption by endogenous chromophores is reduced, yet absorption by water is still negligible. This paves the way for deeper penetration of light into tissue with reduced attenuation¹². Optogenetic tools to manipulate neuronal activity should ideally be excited by near-infrared light. Current development of ChRs has produced many new variants that are maximally activated by blue and green light, such as ChR2^{H134R}, ChETA, TC, SFO^{D156A}, ChD, oChEF, oChIEF, CatCh and ChRGR^{7,8,10,17,18,28,29}. Many of these variants have improved properties regarding kinetics, expression and amounts of desensitization compared with native ChR2. However, there has been little progress in the development of red-shifted ChRs.

In this study, we engineered two red-shifted ChR variants, VCOMET and ReaChR, that had strong membrane expression in mammalian cells. The ReaChR variant responded strongly to red light, with a secondary steady-state spectral peak at 630 nm in addition to a primary steady-state spectral peak at ~540 nm. The mechanism for this shift involves the L171I mutation in VCOMET. Past work attributed this position to the red shift of the response spectrum of VChR1 (Leu126) relative to ChR2 (Ile131)¹⁴, which implies that this L171I modification should lead to a blue shift in the response spectrum. However, this idea is based on the charge distribution of all-*trans* retinal in the binding pocket of bacteriorhodopsin in the dark state. In bacteriorhodopsin, some transient intermediate photocycle states have absorption spectra above 600 nm, whereas the initial activation of the protein has a λ_{\max} value of ~570 nm³⁰. It seems that the main effect of the L171I mutation in ReaChR is to extend the lifetime of the red-shifted transient states and reduce the desensitization of the transient state, leading to a greater photocurrent to red light. In support of this hypothesis, we found differential spectral peaks with the transient and steady-state responses of C-VChR1 and VCOMET, with the transient states having λ_{\max} values of ~570–590 nm and the steady-state having a λ_{\max} value of ~530 nm (**Fig. 1f** and **Supplementary Fig. 2b**).

The initially described red-shifted ChR, VChR1, does not express well in mammalian cells and traffics poorly to the membrane, limiting its utility for *in vivo* applications^{14,15}. The recently published variant CIV1 and its derivatives have been reported to have improved expression, membrane trafficking and kinetic properties compared to VChR1 (ref. 11). However, in our tests, CIV1 and its variants were still limited in their membrane trafficking and expression compared to VCOMET and ReaChR, in addition to having slower channel kinetics

(Figs. 1 and 2). The most red-shifted C1V1 derivative, C1V1^{E122T}, has a spectral peak at ~600 nm and slower channel kinetics and limited expression compared with ReaChR (Figs. 1–3). The E122T mutation variant also has a reduced photocurrent, as has been previously reported¹¹, that may result from the position of this residue within the putative channel pore of ChR, as predicted from the crystal structure of ChEF³¹. Thus, the reduction of C1V1^{E122T} photocurrents and slow kinetics negate the spectral advantage that the E122T mutation provides. In contrast, ReaChR is strongly expressed, consistently traffics to the membrane and can be used to reliably trigger temporally precise spiking.

Although ReaChR has an improved spectral response to light at wavelengths greater than 600 nm, it still suffers slow kinetics in its channel closure rate compared to variants such as ChR2, ChIEF, ChD and ChETA^{7,8,10,17,18,28,29}. In the blue light-activated ChR variants, single point mutations that improve the channel kinetics also reduce the channel's light sensitivity^{7,15}. The other known ChR mutation that increased the channel kinetics, E123T of ChR2, E162T of C1V1 and E163T of VCOMET, does so at the expense of reduced light sensitivity and reduced photocurrents¹⁷. In the context of ReaChR, this E-to-t mutation increases the channel kinetics (off rate <30 ms) and surpasses C1V1^{E162T} in terms of kinetics¹¹ but blue shifts the spectral peak to 550 nm (Supplementary Fig. 8) and increases the desensitization of the channel. We did not find incorporation of this mutation useful in the current development of ReaChR. Important future goals in developing red-shifted ChR should include improving light sensitivities and faster kinetics simultaneously and reducing the activation of these variants by light below 500 nm to allow for the independent manipulation of two populations of neurons with two different wavelengths of light.

We were able to exploit the spectral advantages of ReaChR to achieve efficient activation of expressing neurons through fur, skin and intact bone of adult mice with red-orange (617 nm), red (627 nm) and even far-red (655 nm) light (Figs. 5 and 6). This enables new *in vivo* applications of transcranial and deep-brain stimulation with optogenetics. Transcranial stimulation is essential for many chronic studies, as cranial windows can lead to activated microglia and astrocytes as part of an inflammatory response³² that in turn alters neuronal physiology³³ and plasticity³⁴, as well as pial vasculature^{35,36}. Alternatives to our approach for non-invasive transcranial stimulation include clinically approved treatments for several neurological disorders and stroke, such as electroconvulsive therapy, repetitive transcranial magnetic stimulation and transcranial direct-current stimulation. These techniques do not, however, have the spatial and cellular specificity that can be achieved through optogenetics. Thus, optogenetic approaches using red-shifted ChRs, such as ReaChR, have the potential to improve the efficiency of transcranial stimulation to treat neurological disorders.

In the present study, we introduced the ChR ReaChR through injections of an engineered virus directly into the region of interest. In future work, it may be possible to label specific populations of neurons by retrograde transport of ReaChR from a known target^{37,38}. For example, pools of motoneurons in the brainstem or the spinal cord could be labeled by injection into specific muscles rather than into motor nuclei themselves. Such an approach would substantially reduce the invasiveness of an optogenetic strategy for future therapeutic use. Further, one could label opposing muscle groups with short- or long-wavelength ChRs to permit differential optical control of opposing muscle groups. The weak absorption of short wavelengths by ReaChR will not compromise this strategy if the anatomically deeper motor pools are labeled with ReaChR. ReaChR may also facilitate

neurological treatment and neuroprosthetic control through transcranial and possibly transvertebral stimulation.

METHODS

Methods and any associated references are available in the [online version of the paper](#).

Accession codes. Nucleotide sequences for VCOMET and ReaChR have been deposited in the NCBI GenBank nucleotide database under accession codes [KF448070](#) and [KF448069](#), respectively.

Note: Any Supplementary Information and Source Data files are available in the online version of the paper.

ACKNOWLEDGMENTS

J.Y.L. was funded by the Foundation of Research, Science and Technology New Zealand, and P.M.K. was supported by a long-term fellowship from the Human Frontier Science Program (HFSP). The project was supported by grants to R.Y.T. from the US National Institutes of Health (NS027177) and the Howard Hughes Medical Institute and grants to D.K. from the US National Institutes of Health (DA029706, OD006831 and NS058668). We thank P. Tsai for suggesting the name ReaChR. We thank K. Deisseroth (Stanford University) for the hChR2^{H134R}-eYFP construct, K. Svoboda (Howard Hughes Medical Institute Janelia Farm Research Campus) for the CAG promoter vector, E. Boyden (Massachusetts Institute of Technology) for the lentiviral vector, L. Tian (Howard Hughes Medical Institute Janelia Farm Research Campus) for the AAV2 vector and D. Trono (École Polytechnique Fédérale De Lausanne) for the pSPAX2 and pMD2.G lentivirus packaging vectors. AAV2-ReaChR-Citrine and pLenti-ReaChR-Citrine constructs can be requested from <http://tsienlab.ucsd.edu/Samples.htm>.

AUTHOR CONTRIBUTIONS

J.Y.L. designed and developed ReaChR and conducted and analyzed the experiments in HEK293 and neuron cultures. P.M.K. and A.M. conducted and analyzed the *in vivo* experiments. D.K. and R.Y.T. contributed to the design and analysis of the experiments. All authors contributed to the writing and discussions of the manuscripts.

COMPETING FINANCIAL INTERESTS

The authors declare no competing financial interests.

Reprints and permissions information is available online at <http://www.nature.com/reprints/index.html>.

- Arrenberg, A.B., Stainer, D.Y., Baier, H. & Huisken, J. Optogenetic control of cardiac function. *Science* **330**, 971–974 (2010).
- Boyden, E.S., Zhang, F., Bamberg, E., Nagel, G. & Deisseroth, K. Millisecond-timescale, genetically targeted optical control of neural activity. *Nat. Neurosci.* **8**, 1263–1268 (2005).
- Bruegmann, T. *et al.* Optogenetic control of heart muscle *in vitro* and *in vivo*. *Nat. Methods* **7**, 897–900 (2010).
- Nagel, G. *et al.* Channelrhodopsin-1: a light-gated proton channel in green algae. *Science* **296**, 2395–2398 (2002).
- Nagel, G. *et al.* Channelrhodopsin-2, a directly light-gated cation-selective membrane channel. *Proc. Natl. Acad. Sci. USA* **100**, 13940–13945 (2003).
- Adamantidis, A.R., Zhang, F., Aravanis, A.M., Deisseroth, K. & de Lecea, L. Neural substrates of awakening probed with optogenetic control of hypocretin neurons. *Nature* **450**, 420–424 (2007).
- Lin, J.Y., Lin, M.Z., Steinbach, P. & Tsien, R.Y. Characterization of engineered channelrhodopsin variants with improved properties and kinetics. *Biophys. J.* **96**, 1803–1814 (2009).
- Wen, L. *et al.* Opto-current-clamp actuation of cortical neurons using a strategically designed channelrhodopsin. *PLoS ONE* **5**, e12893 (2010).
- Govorunova, E.G., Spudich, E.N., Lane, C.E., Sineshchekov, O.A. & Spudich, J.L. New channelrhodopsin with a red-shifted spectrum and rapid kinetics from *Mesostigma viride*. *MBio*. **2**, e00115–e001111 (2011).
- Kleinlogel, S. *et al.* Ultra light-sensitive and fast neuronal activation with the Ca²⁺-permeable channelrhodopsin CatCh. *Nat. Neurosci.* **14**, 513–518 (2011).
- Yizhar, O. *et al.* Neocortical excitation/inhibition balance in information processing and social dysfunction. *Nature* **477**, 171–178 (2011).
- Tromberg, B.J. *et al.* Non-invasive *in vivo* characterization of breast tumors using photon migration spectroscopy. *Neoplasia* **2**, 26–40 (2000).
- Aravanis, A.M. *et al.* An optical neural interface: *in vivo* control of rodent motor cortex with integrated fiberoptic and optogenetic technology. *J. Neural Eng.* **4**, S143–S156 (2007).

14. Zhang, F. *et al.* Red-shifted optogenetic excitation: a tool for fast neural control derived from *Volvox carteri*. *Nat. Neurosci.* **11**, 631–633 (2008).
15. Lin, J.Y. A user's guide to channelrhodopsin variants: features, limitations and future developments. *Exp. Physiol.* **96**, 19–25 (2011).
16. Wang, H. *et al.* Molecular determinants differentiating photocurrent properties of two channelrhodopsins from *Chlamydomonas*. *J. Biol. Chem.* **284**, 5685–5696 (2009).
17. Gunaydin, L.A. *et al.* Ultrafast optogenetic control. *Nat. Neurosci.* **13**, 387–392 (2010).
18. Nagel, G. *et al.* Light activation of channelrhodopsin-2 in excitable cells of *Caenorhabditis elegans* triggers rapid behavioral responses. *Curr. Biol.* **15**, 2279–2284 (2005).
19. Griesbeck, O., Baird, G.S., Campbell, R.E., Zacharias, D.A. & Tsien, R.Y. Reducing the environmental sensitivity of yellow fluorescent protein. Mechanism and applications. *J. Biol. Chem.* **276**, 29188–29194 (2001).
20. Mattis, J. *et al.* Principles for applying optogenetic tools derived from direct comparative analysis of microbial opsins. *Nat. Methods* **9**, 159–172 (2012).
21. Hill, D.N., Curtis, J.C., Moore, J.D. & Kleinfeld, D. Primary motor cortex reports efferent control of vibrissa motion on multiple timescales. *Neuron* **72**, 344–356 (2011).
22. Berg, R.W. & Kleinfeld, D. Vibrissa movement elicited by rhythmic electrical microstimulation to motor cortex in the aroused rat mimics exploratory whisking. *J. Neurophysiol.* **90**, 2950–2963 (2003).
23. Brecht, M., Schneider, M., Sakmann, B. & Margrie, T.W. Whisker movements evoked by stimulation of single pyramidal cells in rat motor cortex. *Nature* **427**, 704–710 (2004).
24. Haiss, F. & Schwarz, C. Spatial segregation of different modes of movement control in the whisker representation of rat primary motor cortex. *J. Neurosci.* **25**, 1579–1587 (2005).
25. Herfst, L.J. & Brecht, M. Whisker movements evoked by stimulation of single motor neurons in the facial nucleus of the rat. *J. Neurophysiol.* **99**, 2821–2832 (2008).
26. Martin, M.R. & Lodge, D. Morphology of the facial nucleus of the rat. *Brain Res.* **123**, 1–12 (1977).
27. Dörfel, J. The musculature of the mystacial vibrissae of the white mouse. *J. Anat.* **135**, 147–154 (1982).
28. Berndt, A., Yizhar, O., Gunaydin, L.A., Hegemann, P. & Deisseroth, K. Bi-stable neural state switches. *Nat. Neurosci.* **12**, 229–234 (2009).
29. Berndt, A. *et al.* High-efficiency channelrhodopsins for fast neuronal stimulation at low light levels. *Proc. Natl. Acad. Sci. USA* **108**, 7595–7600 (2011).
30. Shichida, Y., Matuoka, S., Hidaka, Y. & Yoshizawa, T. Absorption spectra of bacteriorhodopsin measured by laser photolysis at room temperatures. *Biochim. Biophys. Acta* **723**, 240–246 (1983).
31. Kato, H.E. *et al.* Crystal structure of the channelrhodopsin light-gated cation channel. *Nature* **482**, 369–374 (2012).
32. Xu, H.T., Pan, F., Yang, G. & Gan, W.B. Choice of cranial window type for *in vivo* imaging affects dendritic spine turnover in the cortex. *Nat. Neurosci.* **10**, 549–551 (2007).
33. Hauss-Wegrzyniak, B., Lynch, M.A., Vraniak, P.D. & Wenk, G.L. Chronic brain inflammation results in cell loss in the entorhinal cortex and impaired LTP in perforant path-granule cell synapses. *Exp. Neurol.* **176**, 336–341 (2002).
34. Grutzendler, J., Kasthuri, N. & Gan, W.B. Long-term dendritic spine stability in the adult cortex. *Nature* **420**, 812–816 (2002).
35. Sohler, T.P., Lothrop, G.N. & Forbes, H.S. The poial circulation of normal, non-anesthetized animals. Part 1. Description of a method of observation. *J. Pharmacol. Exp. Ther.* **71**, 325–330 (1941).
36. Drew, P.J. *et al.* Chronic optical access through a polished and reinforced thinned skull. *Nat. Methods* **7**, 981–984 (2010).
37. Gradinaru, V. *et al.* Targeting and readout strategies for fast optical neural control *in vitro* and *in vivo*. *J. Neurosci.* **27**, 14231–14238 (2007).
38. Osakada, F. *et al.* New rabies virus variants for monitoring and manipulating activity and gene expression in defined neural circuits. *Neuron* **71**, 617–631 (2011).



ONLINE METHODS

Molecular cloning and transgene expression. ChR chimeras and point mutants were generated by overlapping PCR with Phusion PCR mix (New England Biolabs, Ipswich, MA, USA). Genes coding mammalian codon-optimized VChR1, VChR2 and ChIEF were synthesized separately according to the published peptide sequence (GenScript, Piscataway, NJ). The gene encoding hChR2^{H134R}-eYFP was a generous gift from K. Deisseroth (Stanford University). The gene and peptide sequences of ReaChR and C1V1^{E122T} are shown in **Supplementary Figures 9 and 10**. Standard digestion and ligation techniques were used to insert the mutant into the expression vector. For experiments with HEK293 cells, the ChR variants were expressed with the pcDNA3.1 vector under the cytomegalovirus (CMV) promoter and fused to the YFP variant Citrine¹⁹ with an in-frame XhoI restriction site (LeuGlu). Cells were transfected with Fugene HD (Roche, Basel, Switzerland). In the experiments measuring membrane expression of hChR2, ChIEF, VChR1, C-VChR1 and VCOMET in primary cultured neurons, ChR-Citrine fusions (with an in-frame ClaI restriction site) were expressed under the CAG promoter with a WPRE (woodchuck hepatitis virus post-transcriptional regulatory element) sequence inserted after the stop codon of the ChR-Citrine coding sequence (plasmid courtesy of K. Svoboda, Janelia Farm Research Campus). In the experiments measuring membrane expression of C1V1^{E122T}, C1V1^{E122T}-TS and ReaChR, ChR-Citrine fusions (with an in-frame XhoI restriction site) were expressed under the hSyn promoter with a WPRE sequence inserted after the stop codon of the ChR-Citrine coding sequence in an AAV2 vector (plasmid courtesy of L. Tian, Howard Hughes Medical Institute Janelia Farm Research Campus). The resulting constructs (at the same DNA concentration) were electroporated into the neurons before plating (Lonza, Walkersville, MD). For the stimulation of cultured primary hippocampal neurons with red light, ReaChR-Citrine was introduced with recombinant lentivirus.

Lentivirus and rAAV production. The genes encoding hChR2^{H134R}-eYFP, C1V1^{E122T}-TS-Citrine, oChIEF-Citrine and ReaChR-Citrine were subcloned into a generation-two lentiviral construct with the hSyn promoter. The lentivirus was made according to the protocols at <http://vectorcore.salk.edu/protocols.php> with minor modifications. In brief, 293A cells (Life Technologies, Carlsbad, CA) were grown to 85% confluency, and transfer vectors containing ChR-fluorescent protein, psPAX2 and pMD2.G (gifts from D. Trono, École Polytechnique Fédérale De Lausanne) were transfected with calcium phosphate (Clontech, Mountainview, CA). Virus particles were harvested from serum-free medium and concentrated with a 20% sucrose cushion with ultracentrifugation. The titer of the lentivirus was estimated with the Lentivirus Rapid Quantitation Kit (Cell Biolabs Inc. San Diego, CA) in parallel just before each infection. The lentiviral vector was a gift from E. Boyden (Massachusetts Institute of Technology). rAAV with serotype 8 containing hChR2^{E134R}-eYFP and ReaChR-Citrine was produced and purified according to the protocols at <http://vectorcore.salk.edu/protocols.php> by transfecting an AAV2 inverted terminal repeat (ITR) vector (gift from L. Tian, Howard Hughes Medical Institute Janelia Farm Research Campus) containing ReaChR-Citrine and the helper plasmids XX6-80 and XR8 (National Vector Biorepository) into 293A cells. rAAV2/8 (recombinant AAV serotype 8 packaged with AAV2 ITR) were released from the cells by freeze thawing and purified with iodixanol gradient purification. The virus was further concentrated using an Amicon Ultra centrifugal filter (Millipore, Billerica, MA) with a 50 kDa cutoff. The rAAV titer was measured by the Salk Vectorcore service with quantitative PCR and was estimated to be 3×10^{13} GC ml⁻¹.

Measurement of relative efficiencies of ChR membrane expression. Relative levels of plasma membrane expression of ChR-Citrine fusions in HEK293 and cultured cortical neurons were measured by imaging on a Zeiss Live 5 Confocal microscope with Zen software (Thornwood, NY). Transfections and measurements of expression were performed with the same concentrations of DNA electroporated into the neurons. The transfected cells were imaged with the same setting for comparison. The measurements of expression were performed on all cells with detectable visible fluorescence and normal cell morphology non-discriminatively in the culture dish to ensure fair comparisons, typically starting from one end of the dish and moving to the other. Membrane expressions were measured by taking the mean fluorescence intensities of the membrane and the cytosol of a single in-focus imaging plane with ImageJ software. In the experiments in which ChR photocurrents were normalized to the membrane fluorescence,

images were acquired with an electron multiplying charge-coupled device (EMCCD) camera (Photometric, Tucson, AZ) at a 512 × 512 pixel resolution with Slidebook (Intelligent Imaging Innovations, Inc., Denver, CO) in epifluorescence mode before electrophysiological recordings.

Cell culture, electrophysiological recordings and stimulation of cultured cells.

Characterization of spectral responses, reversal potentials, kinetics and membrane trafficking of C-VChR1, C1V1, C1V1^{E122T}, VCOMET, ReaChR, CatCh, oChIEF and oChEF were done with whole-cell patch clamping on 293A cells 2 d after transfection. HEK293 cells, which have a smaller size, high membrane resistance and minimal expression of voltage-gated ion channels, were used for these characterizations to reduce the known voltage-clamping errors in neurons³⁹. All recordings were performed with an extracellular solution containing 118 mM NaCl, 3 mM KCl, 2 mM CaCl₂, 1 mM MgCl₂, 10 mM 4-(2-hydroxyethyl)-1-piperazineethanesulfonic acid (HEPES), 20 mM glucose (pH 7.35, 310 mOsm) and an intracellular solution containing 110 mM Cs-methanesulfonate, 30 mM tetraethylammonium chloride, 10 mM ethylene glycol tetraacetic acid (EGTA), 10 mM HEPES, 1 mM CaCl₂, 1 mM MgCl₂, 2 mM Mg-ATP and 0.15 mM Na₃-GTP (pH 7.25, 285 mOsm), except for the reversal-potential measurements, for which the intracellular solution contained 125 mM K-gluconate, 10 mM K₄-1,2-bis-(*o*-aminophenoxy)-ethane-*N,N,N',N'*-tetraacetic acid (BAPTA), 5 mM NaCl, 1 mM CaCl₂, 10 mM HEPES, 2 mM Mg-ATP and 0.3 mM Tris-GTP (pH 7.25, 285 mOsm). Series resistance compensation (at 70–75%) was used in the kinetics and reversal-potential measurements in HEK293 cells. HEK293 cells with low membrane resistance (<200 MΩ) were often discarded from analysis and testing because of the inaccuracy of voltage clamping in these conditions. These cells are typically found in clusters. All chemicals were acquired from Sigma-Aldrich (St. Louis, MO). Electrophysiological characterization of ChR in neurons were performed on *in vitro* day 14–25 neurons extracted from postnatal day 2 neonatal Sprague-Dawley rat pups (both sexes were used, and the neurons were pooled together for the culture) after at least 9 d of infection with lentivirus. For the measurement of photocurrent amplitudes in neurons, the recordings were performed with Cs-methanesulfonate-based intracellular solution to block the potassium channel, and 1 μM tetrodotoxin and 100 μM Cd²⁺ were included in the extracellular solution to block voltage-gated sodium and calcium channels, respectively. Also included in the extracellular solution were 10 μM NBQX (6-nitro-2,3-dioxo-1,4-dihydrobenzo[*f*]quinoxaline-7-sulfonamide), 10 μM bicuculline and 20 μM AP5(D(-)-2-amino-5-phosphonovaleric acid) to block fast synaptic transmission (Tocris, Ellisville, MO). To ensure the accuracy of the voltage clamping in neurons, light illumination was limited to a circular area of 150 μm diameter around the soma to reduce space-clamp error, and series resistance was compensated at 65%. Four-hundred-seventy nanometer light was used to activate hChR2^{H134R} and oChIEF for photocurrent measurements, and 590 nm light was used for C1V1^{E122T}-TS and ReaChR. Although the experimenters were not blinded to groups, the cells tested were selected on the basis of a healthy appearance under bright-field illumination without visualization of fluorescence to ensure unbiased selection. All cells tested were included in the analysis regardless of detectable responses to light. For testing the effectiveness of light in evoking action potentials, the recordings were performed with a K-gluconate-based intracellular solution in the presence of extracellular 10 μM NBQX, 10 μM bicuculline and 20 μM AP5. Recordings were performed in current-clamp mode with the current injected to sustain a -65 mV membrane potential at rest. In pulsed stimulation experiments, cells that did not reach suprathreshold depolarization with 20 ms of 50 mW mm⁻² light pulses were excluded from the analysis. For experiments of neurons with 10 Hz stimulation under the current clamp, ReaChR-Citrine- and oChIEF-Citrine-expressing cells were selected on the basis of bright-field morphology without visualization with fluorescence. High membrane eYFP fluorescence was used to select hChR2^{H134R} cells for recordings, as most cells with medium to low levels of fluorescence did not reach the threshold when stimulated with light. Recordings were performed with the Axopatch 200B patch clamp amplifier (Molecular Devices, Union City, CA) and acquired through Digidata 1320 (Molecular Devices) to a personal computer (Dell, Austin, TX) running pClamp 9.2 or pClamp 10 software (Molecular Devices). Analyses were conducted with AxographX (Sydney, New South Wales, Australia). Junction potentials were not corrected.

Most light stimulation was provided by a monochromator xenon light source (Polychrome IV, TILL Photonics, Victor, NY) with 15 nm half width.

The shuttering and intensity of the light were controlled with a custom-fitted 25 mm mechanical shutter (Vincent Associates, Rochester, NY) and a neutral density wheel (Thorlab, Newton, NJ). For the spectral response measurements and experiments in which the light intensity was not described, cells were stimulated with $\sim 5.1 \times 10^{16}$ photon $\text{mm}^{-2} \text{s}^{-1}$ across the light spectra. The photon flux of the monochromator at each wavelength was measured with a power meter and integrating sphere (Newport Corporation, Irvine, CA) placed on the objective, and the photon flux was corrected with the neutral density wheel to give the same flux. The response spectra of the ChRs were measured with a 1 s light pulse from 650 to 410 nm of the same photon flux at 20 nm intervals, with the maximum response taken as the maximal photocurrent obtained within the 1 s pulse at the described wavelength, and the steady-state response was measured between 0.95–1.00 s after the onset of the stimulation light pulse. For most experiments, 410 nm light was delivered 20 s after the initial stimulation to recondition the protein before the delivery of the next testing pulse 20 s later. Stimulation of neurons under the current clamp was conducted with 470 nm (SR-05-B0040), 617 nm (SR-05-H2070) or 627 nm (SR-05-D2050) LED illumination (Luxeonstar, Brantford, Ontario, Canada). The LEDs were connected to a computer-controlled current source (Mightex, Pleasanton, CA) coupled to a quartz fiber into the microscope.

Expression and stimulation of ChR-expressing neurons *in vivo*. Recombinant AAV2/8-hSyn-ReaChR-Citrine or AAV2/8-hSyn-hChR2^{H134R}-eYFP virus was injected stereotaxically into the vibrissa motor cortex (vM1) or the facial motor nucleus in the brainstem of C57BL/6 female mice using a nanoliter injector (Nanoject II, Drummond, Broomall, PA) under isoflurane anesthesia (2% (vol/vol)). The injection coordinates for vM1 were 1 mm posterior, 1 mm lateral and 0.8 mm ventral, and the coordinates for the facial motor nucleus were 4.8–5.6 mm posterior, 1.2–1.4 mm medial and 5.3–6.0 mm ventral to the bregma. The skin was retracted to expose the injection coordinates, and a single 0.3 mm diameter hole was drilled for each injection site. Suspension of virus was injected in ten 50 nl aliquots every 5 min (total volume, 500 μl) in vM1 and in five 12 μl aliquots (total volume, 60 μl) every 5 min in the facial motor nucleus. The injection hole was filled with sterile saline and topped with a thin layer of antibiotic ointment after the injection pipette was withdrawn. The skin was sutured back in place, and the mouse was left to recover for the viral incubation period. After a waiting period of 4 weeks, the mice were prepared for *in vivo* experiments. The injections of virus were done on 3-month-old mice, and the tests were performed 3–6 weeks later. All mice were housed on a normal 12 h light, 12 h dark cycle in groups of between 3 and 5 mice per cage, and all mice were tested during the light cycle.

One day before the experiments, a single 10 mm incision was made perpendicular to the midline and caudal to lambda, the skull was exposed, and a titanium alloy head bar was attached to the skull using cyanoacrylate gel and a layer of dental cement (C&B-Metabond, Parkell Inc., Edgewood, NY) during isoflurane anesthesia. The skin rostral to the lambda was not damaged, and the skull under it was neither exposed nor covered by any amount of cement, except for during the electrophysiological recordings in vM1, for which a new craniotomy was opened

where the virus had been injected previously. Over the next several days mice were head fixed either when awake or during isoflurane anesthesia (0.5–2%), as indicated. ReaChR was activated *in vivo* by LEDs with wavelengths of 470 nm (LXML-PB01-0030), 530 nm (LXML-PM01-0100), 591 nm (LXM2-PL01-0000), 617 nm (LXM2-PH01-0070), 627 nm (LXM2-PD01-0050) and 655 nm (LXM3-PD01-0260, Luxeonstar, Brantford, Ontario, Canada) connected to a computer-controlled current source (Mightex, Pleasanton, CA).

Single units in vM1 and the facial motor nucleus were recorded extracellularly with 9–12 M Ω tungsten electrodes (UEWLCSMLN1G, FHC Inc., Bowdoin, ME), buffered, preamplified (Alpha Omega Co., Alpharetta, GA) and acquired onto a personal computer (PCIe-6361, National Instruments, Austin, TX) using custom-written software for Matlab (MathWorks, Natick, MA). Spikes were sorted using the Chronux library in Matlab (<http://chronux.org>).

Vibrissa movements were monitored with high-speed video³⁶ and tracked offline using the WhiskerTracker software⁴⁰ (code available at <https://github.com/pmknutsen/whiskertracker>). After *in vivo* experiments, the mice were perfused with 4% paraformaldehyde, the brains were extracted, and ReaChR expression was confirmed with epifluorescence imaging and localized histologically using a fluorescent Nissl counterstain (NeuroTrace N21479, Life Technologies, Carlsbad, CA). The bone overlying the injection sites was inspected after perfusions and was invariably found to have regrown entirely. In most mice, the bone that had regrown after viral injections appeared thickened. Only mice with ChR expression in the correct regions identified with postmortem histochemical analysis were included in the analysis of spiking and vibrissa movement. Although the experimenter was not blinded to group status, the measurement was automated, so blinding status would not affect the outcome of the experiment. All animal procedures, including the extraction of primary neurons, were approved by the UCSD Institutional Animal Care and Use Committee.

Statistical analyses. Comparisons of the properties of ChR variants in culture were done by nonparametric Kruskal-Wallis test with *post-hoc* Dunn's multiple comparison tests between all possible pairs. Only the *P* values for the Kruskal-Wallis tests are shown. The statistical analyses were done with Graphpad Prism 5.0 (San Diego, CA). The comparisons *in vivo* were conducted with nonparametric one-sided Kolmogorov-Smirnov tests in Matlab. All values are presented as the mean \pm s.e.m. All data in the graphs are presented as the mean \pm s.e.m., with the exception of the 10 Hz stimulation experiments and spike latency analysis, in which the s.d. is shown to illustrate the variability. No statistical methods were used to predetermine sample sizes, but our sample sizes were similar to those reported in previous publications^{7,20}. Most analyses in cultured cells were summarized from multiple transfection or transduction experiments. The full results of the statistical analyses are available in **Supplementary Data Set 1**.

39. Armstrong, C.M. & Gilly, W.F. Access resistance and space clamp problems associated with whole-cell patch clamping. *Methods Enzymol.* **207**, 100–122 (1992).

40. Knutsen, P.M., Derdikman, D. & Ahissar, E. Tracking whisker and head movements in unrestrained behaving rodents. *J. Neurophysiol.* **93**, 2294–2301 (2005).